IET Microwaves, Antennas & Propagation

Research Article

IET Journals
The Institution of Engineering and Technology

Antenna design based on quasi-degenerate characteristic modes of unbroken metal rim

ISSN 1751-8725
Received on 8th March 2017
Revised 6th August 2017
Accepted on 18th August 2017
E-First on 27th September 2017
doi: 10.1049/iet-map.2017.0192
www.ietdl.org

Longyue Qu[1], Jihwan Jeon[1], Donghee Park[1], Hyeongdong Kim[1] ✉

[1]*Department of Electronics and Computer Engineering, Hanyang University, 222 Wangsimni-ro, Seongdong-gu, Seoul, Republic of Korea*
✉ *E-mail: hdkim@hanyang.ac.kr*

Abstract: A simple and efficient antenna technique for both single antenna and multiple-input multiple-output (MIMO) antenna design utilising an unbroken metal rim is analysed in the frequency band <1 GHz for mobile phone applications. A 110 mm × 55 mm × 5 mm unbroken metal rim has two characteristic modes (Modes 1 and 2) that resonate around 1 GHz, and these two modes are quasi-degenerate and orthogonal to each other. An uncontacting feeding structure is proposed to excite and utilise the characteristic modes of the unbroken metal rim for antenna radiation. In MIMO antenna design, it is possible to achieve high isolation and good diversity performance by properly exciting orthogonal modes with the proposed feeding technique. Two different cases for MIMO designs are presented to verify the feasibility of the proposed technique. In both two cases, the simulated isolation is ∼10 dB, and the 3:1 VSWR bandwidths for the MIMO antennas are wider than 150 and 60 MHz, respectively. The measured results show that the envelope correlation coefficients for each case are <0.2, indicating good diversity performance. The measured radiation patterns for the two MIMO antennas are orthogonal, again verifying the diversity performance.

1 Introduction

Recently, metal rims have been widely adopted in smartphones due to mechanical considerations and the need of customers. In general, metal rims have two kinds of configurations: broken and unbroken, which commonly cause antenna performance problems, such as narrow matching and reduced efficiency [1, 2]. However, this effect can be reduced by proper designs [1–5], and the metal rims can even be utilised as radiators [6–9] while achieving good radiation performance and saving space in printed circuit boards (PCBs). Of these studies, the most popular technique involves inserting grounding patches/points between the metal rim and the ground plane to build slot/loop-type resonators [2–4]. Another technique that was proposed uses the metal rims as radiators by introducing open gaps or slits in the rims [6–9].

These reference studies provided promising candidates for single antenna designs in the presence of metal rims. However, achieving a multiple-input multiple-output (MIMO) antenna design is still a big challenge. High isolation and low envelope correlation coefficients (ECCs) are required for MIMO applications, since good diversity performance is essential for enhancing the community capacity for high-speed data transmission in MIMO technology [10]. The PCBs are small compared with the wavelength. Therefore, there is strong mutual coupling, especially in the low-frequency band, resulting in bad isolation and low efficiency. Even though various decoupling techniques have been presented, e.g. such as additional resonators [11–14] and decoupling networks [15, 16], they are not practical to implement in the low-frequency band. Orthogonal or diagonal mode excitation presented in [17–19] provides us an interesting insight that characteristic mode theory can be a useful tool for solving metal-rimmed MIMO design problems. Recent studies on metal rim MIMO antennas were presented in [20–23]. Low correlated MIMO antennas are proposed in [20, 21] by exciting the bezel mode and the chassis mode, respectively. However, the matching networks as well as chassis modification are difficult to achieve in [20], and large occupation as well as wide gap between the ground plane and the metal rim are required in [21], restricting their practical applications. In [22], characteristic modes are controlled and utilised for wideband applications of MIMO antennas, but four gaps in the metal rims and two connection pins are needed, which can be difficult in implementation. Besides, MIMO antennas are presented by using double-ring structure in [23], and the main drawbacks can be its large area and strong mutual coupling.

A simple and efficient MIMO technique with good diversity performance is required for devices with unbroken metal rims. The main contribution of this paper is that quasi-degenerate (approximately the same resonant frequencies) characteristic modes in the unbroken metal rim can be excited by a simple and efficient feeding structure, and they can be excited and utilised for MIMO antenna applications to achieve high isolation and low ECC performance. Meanwhile, the feeding structure is non-contacting to the metal rim, which can be favourable in practical applications. More importantly, this study provides interesting insight and another possible antenna design for unbroken metal rim antennas. Using the proposed technique, we designed a compact antenna that showed wideband, high isolation and low ECC in the frequency band <1 GHz. Our goal was to present a novel technique for both single antenna and MIMO antenna design, so this initial study was verified in the low-frequency band only. However, this technique can be easily extended to high-frequency bands. It is noted that all simulation is conducted by using High Frequency Simulator Software.

2 Modal analysis and single antenna design

2.1 Modal analysis of unbroken metal rim

The theory of characteristic modes is an important tool for antenna design, especially for mobile antennas. Accordingly, $\boldsymbol{J}_n$ is usually used for the characteristic current of the nth mode, characterised by the shape of an arbitrary conducting body. α_n is the modal excitation coefficient, representing the magnitude to which degree a characteristic mode is excited by the external excitation [24, 25]. The total current distribution on the surface of the conducting body can be expressed a linear summation of modal currents with various coefficients as

$$\boldsymbol{J} = \sum_n \alpha_n \boldsymbol{J}_n \tag{1}$$

where

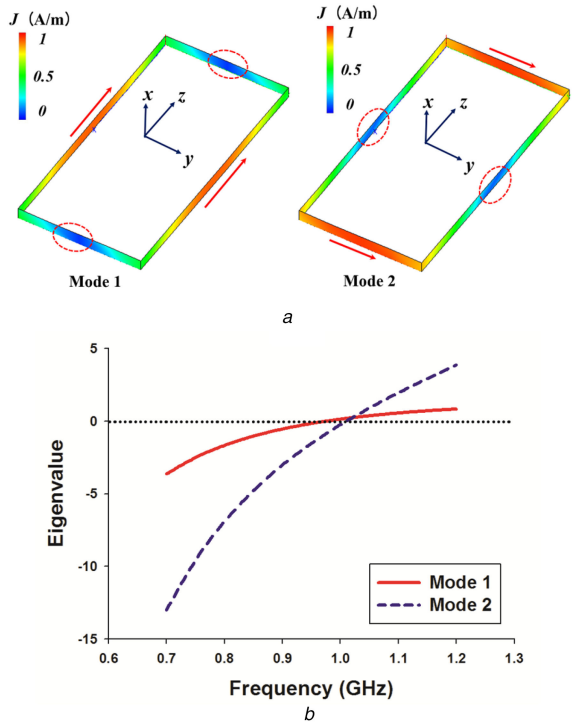

Fig. 1 *Analysis of 110 mm × 55 mm × 5 mm unbroken metal rim*
(a) Normalised characteristic currents, ***(b)*** Eigenvalues

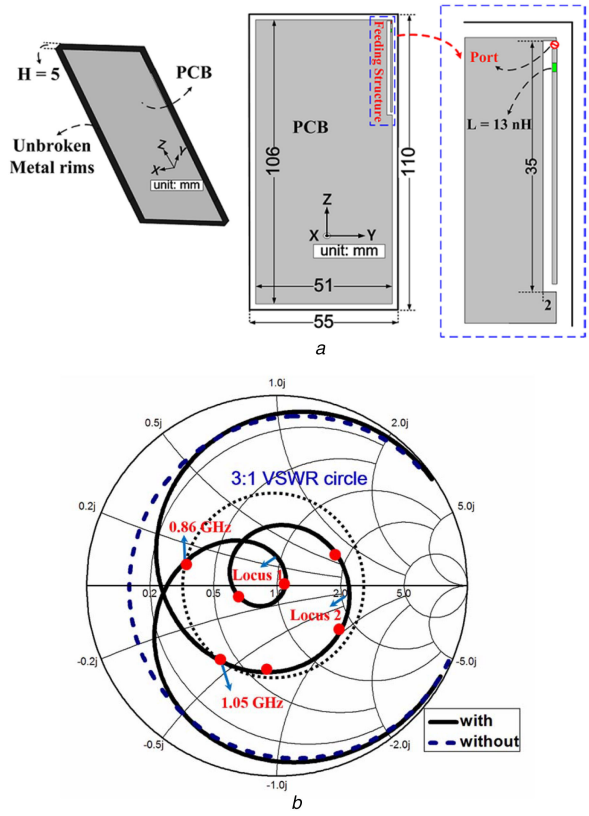

Fig. 2 *Single antenna design using unbroken metal rim*
(a) Geometry of the proposed single antenna design, ***(b)*** Input impedance in a Smith chart with and without the metal rim

$$\alpha_n = \frac{\int\int\int (\boldsymbol{E}_n \cdot \boldsymbol{J}_a)\mathrm{d}\tau}{1 + j\lambda_n} \text{ or } \frac{-\int\int\int (\boldsymbol{H}_n \cdot \boldsymbol{M}_a)\mathrm{d}\tau}{1 + j\lambda_n} \quad (2)$$

In (2), $\boldsymbol{E}_n$ and $\boldsymbol{H}_n$ are the characteristic electric and magnetic field generated by the characteristic current $\boldsymbol{J}_n$. $\boldsymbol{J}_a$ and $\boldsymbol{M}_a$ are the electric-type current and magnetic-type current produced by the antenna, respectively. The numerator in (2) is defined as the reaction or coupling. In the denominator, λ_n is the eigenvalue, and it is zero if $\omega = \omega_n$, where ω_n is the resonant frequency of the nth mode, so that α_n approaches its maximum at resonance of the characteristic mode. Therefore, the total current distribution over the surface of the conducting body is determined by both the eigenvalue λ_n and the coupling.

In Fig. 1*a*, an unbroken metal rim with dimensions of 110 mm (length) × 55 mm (width) × 5 mm (height) that is frequently used in smartphones is presented, and its characteristic modes without the PCB is illustrated for simple analysis. Fig. 1*b* provides the eigenvalues (λ_1 and λ_2) of the two current modes ($\boldsymbol{J}_1$ and $\boldsymbol{J}_2$) which resonate around 1 GHz. Their corresponding normalised characteristic currents are plotted in Fig. 1*a*. As shown, the current distributions of both modes work as one-wavelength loop-type resonators along one circle of the metal rim with sinusoidal current distributions, and two nulls are circled in Fig. 1*a*. Meanwhile, it is evident that their radiation patterns are orthogonal to each other, according to the orthogonality relationship of the theory of characteristic modes. Furthermore, Mode 1 exhibits better radiating bandwidth and radiation characteristics than Mode 2, which is consistent with the eigenvalue behaviour, i.e. the slope of the curve at resonance in Fig. 1*b*.

Furthermore, Modes 1 and 2 have approximately the same resonant frequencies since the physical dipole lengths are the same, but slightly different in effective lengths because of their different shapes, which can be expected. For totally symmetrical structures, e.g. circular loops, square loops or spheres, degenerate modes can be generated with the same current distribution and a phase rotation of 90° at the same frequency [25]. In the case of the rectangular metal rim, Modes 1 and 2 are defined as quasi-degenerate modes for simplicity. Therefore, an important character of the unbroken metal rim is its quasi-degenerate and orthogonal characteristic modes. It is noted that the resonant frequencies of both modes can be controlled using various techniques, which is not discussed here. To effectively excite the metal rim as a radiator, simple capacitive coupling (a ***J***-type current at ***E*** field maximum) [26], simple magnetic coupling (an ***M***-type current at ***H*** field maximum) [6, 9, 27] or a combination of capacitive coupling and inductive coupling (a ***J*** and ***M*** mixed-type current at other arbitrary locations) can be considered as in (2). The ***E*** field maximum in Mode 1 is the ***H*** maximum in Mode 2, so each mode can be excited separately. All the characteristics determine that the metal rim itself can be excited and utilised as radiators for both single and MIMO applications.

2.2 Single antenna design

To verify the above analysis on the characteristic modes of the metal rim, a single antenna design is studied. Fig. 2*a* shows the geometry of the proposed single antenna design by using a simple an efficient feeding technique. The 106 mm × 51 mm PCB is printed on a low-cost FR4 substrate with a thickness of 1 mm and dielectric constant $\varepsilon_r = 4.4$. The PCB is surrounded by the unbroken metal rim of 110 mm × 55 mm × 5 mm by a separation gap of 2 mm. The thickness of the metal rims is set as 0.3 mm. Note that the characteristic modes of the metal rim with the PCB are omitted here. Unlike [20, 21], the fundamental characteristic mode of the PCB is out of our consideration, and its effect on the metal rim is assumed to be neglectable.

In Fig. 2*a*, a feeding structure at right-top of the PCB is proposed without any connection between the PCB and the metal rim, so a feeding technique with a ***J*** and ***M*** mixed-type current is adopted to excite the characteristic modes of the metal rim. The proposed feeding structure is designed within a 2 mm × 35 mm clearance, and is fed by a voltage source at the top of a 0.5 mm-width conductor line. A series inductor L (13 nH) is adopted below the source, and the conductor line has a 1 mm gap to the ground plane, so that the resonant frequency of the feeding can be controlled by easily adjusting the values of L or inserting capacitor at the gap. The inductor values as well as optimised results can be obtained when the resonant frequency of the feeding is tuned equal to the operating frequency as well as the metal rim resonance [6, 9, 28] by easily observing the input impedance locus in a Smith chart.

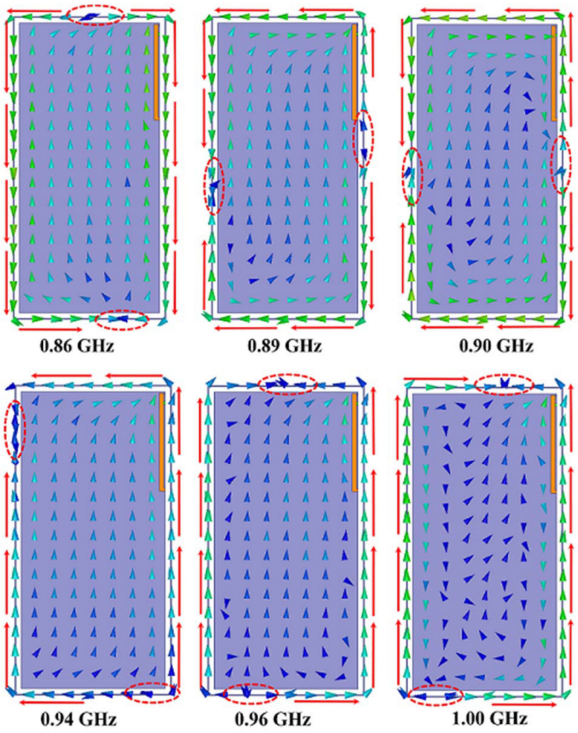

Fig. 3 *Simulated surface current distributions at 0.86, 0.89, 0.90, 0.94, 0.96 and 1 GHz*

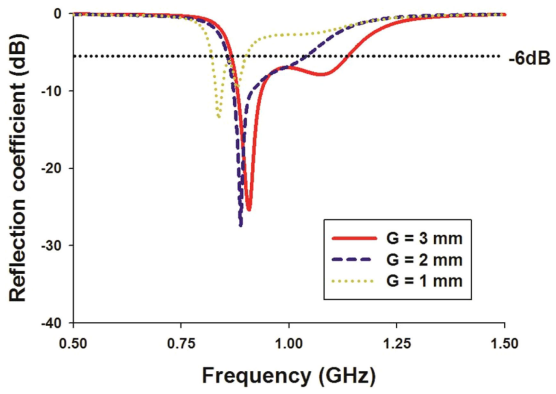

Fig. 4 *Simulated reflection coefficients with gap variation*

The input impedance of the proposed antenna is presented in a Smith chart in Fig. 2*b*, and it can be observed that a 3:1 VSWR bandwidth of 190 MHz (from 0.86 to 1.05 GHz) is obtained. As comparison, the input impedance without the metal rim is also plotted in Fig. 2*b*, which is dominantly reactive, meaning that the antenna with the PCB only contributes little to the radiation loss. Whereas the antenna operates primarily by coupling energy to the metal rim and exciting the metal rim as an effective radiator, so the contribution from coupling between the antenna and the PCB can be neglectable. Furthermore, the modal excitation coefficient is very small when the characteristic modes are not near resonance, as shown in (2), explaining the reasons for little contribution to the antenna radiation performance from other higher modes, including the PCB.

Accordingly, the total current distribution generated by the antenna can be approximately expressed as a combination of Modes 1 and 2, as follows:

$$\boldsymbol{J}_t \simeq \alpha_1 \boldsymbol{J}_1 + \alpha_2 \boldsymbol{J}_2 \tag{3}$$

Based on the values of α_1 and α_2, the total current distributions can be calculated in simulation, which further contribute to the impedance locus in the Smith chart as shown in Fig. 2*b*. One can easily estimate the antenna operating mechanism through the observation of its current distributions. Accordingly, the simulated surface current distributions at 0.86, 0.89, 0.90, 0.94, 0.96 and 1 GHz (circled by red solid dot in Fig. 2*b*) are presented and compared in Fig. 3. As shown, the total current distribution over the metal rim at 0.86, 0.94, 0.96 and 1 GHz is dominantly contributed by Mode 1, whereas those at 0.89 and 0.90 GHz is dominantly due to Mode 2. Accordingly, the small impedance locus (Locus 1) in the Smith chart in Fig. 2*b* is generated mainly by exciting Mode 2, and the large impedance locus (Locus 2) is generated dominantly by excitation of Mode 1. Therefore, the operating mechanism of the proposed antenna can be interpreted as a one-wavelength loop (metal rim) antenna, which is partially filled by the PCB, as can be expected.

One interesting insight is that the direction of current distributions on the PCB is opposite to that in the metal rim due to induction theorem, as shown in Fig. 3. As a result, the opposite flowing current will cancel the current distributions in the metal rim and further degrade the radiation performance. A simple and efficient method of reducing the cancelling effect could be to enlarge the gap between the PCB and the metal rim, which is verified in Fig. 4. Fig. 4 presents the reflection coefficients obtained by changing the gap from 1 to 3 mm, which is achieved by changing the dimensions of the PCB. As shown, the 3:1 VSWR bandwidths vary from 80 MHz (from 0.82 to 0.9 GHz when $G = 1$ mm) to 260 MHz (from 0.87 to 1.13 GHz when $G = 3$ mm).

3 MIMO antenna design

The above analysis has provided interesting insights that the two quasi-degenerate and orthogonal characteristic modes of the metal rim can be effectively utilised for radiation. For MIMO antenna applications, therefore, it is preferred to excite Mode 1 dominantly for Antenna 1, and Mode 2 dominantly for Antenna 2, so that orthogonality and diversity requirement can be sufficiently satisfied. These observations provide us with a simple and efficient MIMO antenna technique. Therefore, it is evident that we can always find two antennas with high isolation and low correlation performance when they are simultaneously exciting the unbroken metal rim, which can be realised by optimising their relative locations and feeding techniques. Based on the proposed single antenna design in Section 2, we present MIMO antenna designs in two cases, and the antenna locations are determined by referring to some popular smartphones, such as Samsung Galaxy, for consideration of its applicability in practical applications. The study cases are presented as possible approaches to address the feasibility of the unbroken metal rim modes in MIMO applications.

In Case 1, Antenna 1 is the same one proposed in Section 2. Antenna 2 is designed with a 1.5 mm × 18 mm feeding structure in the left side of the PCB and is 7 mm away from the upper edge of the PCB as shown in Fig. 5*a*. The feeding structure in Antenna 2 consists of a 0.5 mm conductor line with a series inductor L (45.5 nH) and a 0.5 mm gap at the end. Fig. 5*b* provides the scattering parameters of the proposed MIMO antennas of Case 1. The 3:1 VSWR bandwidths of 150 MHz (from 0.86 to 1.01 GHz) and 60 MHz (from 0.87 to 0.93 GHz) are provided for Antennas 1 and 2, respectively. In the S12 curve, the coupling coefficient ranges from −10.5 to −37 dB in the operating band. Two coupling nulls are generated at 0.8 and 0.95 GHz, respectively. To verify the excited modes, the surface current distributions at 0.89 GHz where maximum coupling coefficient occurs are presented and compared in Fig. 5*c*. Fig. 5*c* is plotted when one antenna is excited with another terminated in a 50 Ω load. For Antenna 1, diagonally directed current distributions are generated with current nulls at the right-top and left-bottom corners of the metal rim, and the current distributions for Antenna 2 are almost the same with those of Mode 2, as shown in Fig. 1*a*. Therefore, it can be obviously observed that Antenna 1 is dominantly coupling with Mode 1, and Antenna 2 is dominantly coupling with Mode 2, which is determined by their locations as well as the feeding techniques.

Case 2 is proposed in Fig. 6*a*, where Antenna 1 is located on the upper side of the PCB within a 2 mm × 30 mm feeding structure and 18 mm away from the left edge of the PCB. Antenna 2 is located on the right side of the PCB, 45 mm away from the lower side of the PCB. The inductor values of L are 20 and 48 nH,

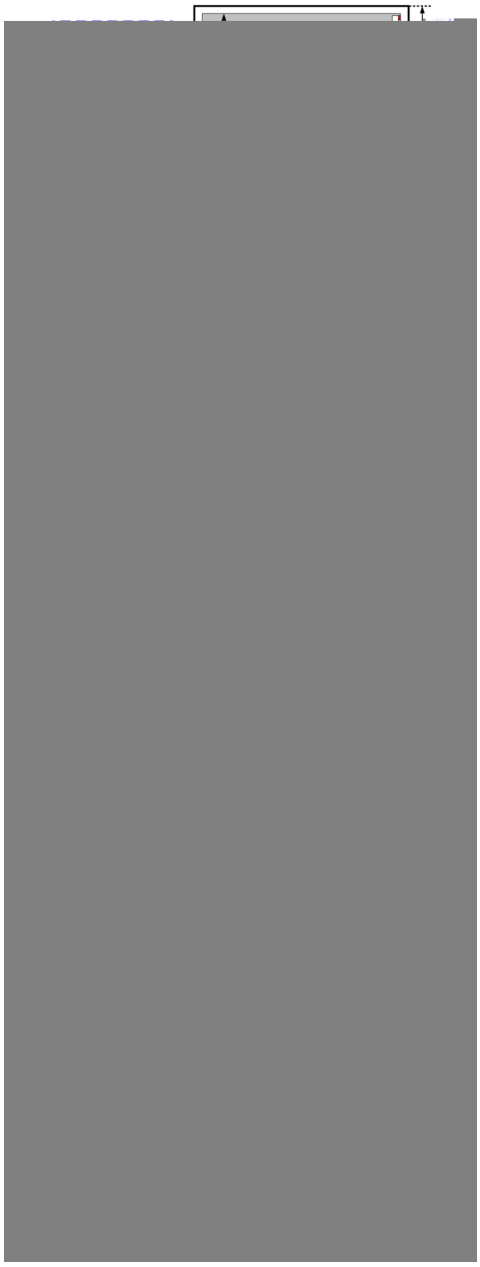

Fig. 5 *MIMO antenna design of Case 1*
(a) Geometry of MIMO antennas, ***(b)*** Simulated *S*-parameters, ***(c)*** Simulated surface current distributions at 0.89 GHz for Antenna 1 excitation (left) and Antenna 2 excitation (right)

Fig. 6 *MIMO antenna design of Case 2*
(a) Geometry of MIMO antennas, ***(b)*** Simulated *S*-parameters, ***(c)*** Simulated surface current distributions at 0.89 GHz for Antenna 1 excitation (left) and Antenna 2 excitation (right)

respectively, and 0.5 mm gaps are adopted at the end of the 0.5 mm conductor line in both feeding structures are adopted. The 3:1 VSWR bandwidths of 160 MHz (from 0.86 to 1.02 GHz) for Antenna 1 and 110 MHz (from 0.86 to 0.97 GHz) for Antenna 2 are obtained, respectively, as shown in Fig. 6*b*. The coupling coefficient is below −9 dB in the operating band. Fig. 6*c* plots the simulated surface current distributions at 0.89 GHz. Antenna 1 generates current distributions that are consistent with those of Mode 1 in Fig. 1*a*, and Antenna 2 produces diagonally directed current distributions with current nulls in the left and right sides of the metal rim. Accordingly, Modes 1 and 2 are primarily excited by Antennas 1 and 2, respectively, verifying the feasibility of the locations of the proposed feeding techniques.

4 Measured results

The metal rim MIMO antennas for all two cases were fabricated as shown in Fig. 7*a*. The antenna performances were measured using an Agilent 8753ES Network analyser in a 6 m × 3 m × 3 m three-dimensional (3D) CTIA Over the Air anechoic chamber. The measured *S*-parameters are plotted in Figs. 7*b* and *c* for each case. For Case 1 in Fig. 7*b*, 3:1 VSWR bandwidths are from 0.80 to 1 GHz and from 0.81 to 0.97 GHz for Antennas 1 and 2, respectively. The isolation between the two antennas is over 17 dB and up to 30 dB at the coupling null over the entire bandwidth. In Case 2, Fig. 7*c*, the measured 3:1 VSWR bandwidths are from 0.775 to 0.99 GHz for Antenna 1 and from 0.785 to 0.92 GHz for Antenna 2 with isolation over 15 dB. The measurements for both two cases are consistent with the simulation results. High isolation and wide bandwidth are achieved both in simulations and measurements by utilising the metal rim modes.

To verify the diversity performance of the proposed MIMO antennas, the measured total radiation efficiencies and ECC are presented in Fig. 8. Since both two cases have similar performances in terms of efficiency and ECC, only the results of Case 1 are shown and investigated. The average efficiency is −2.7 dB (53%), and ranges from −2.4 to −4.1 dB for Antenna 1. For Antenna 2, the efficiency is −4.1 dB (39%), and ranges from −2.8 to −5.9 dB. The performance difference between the two antennas

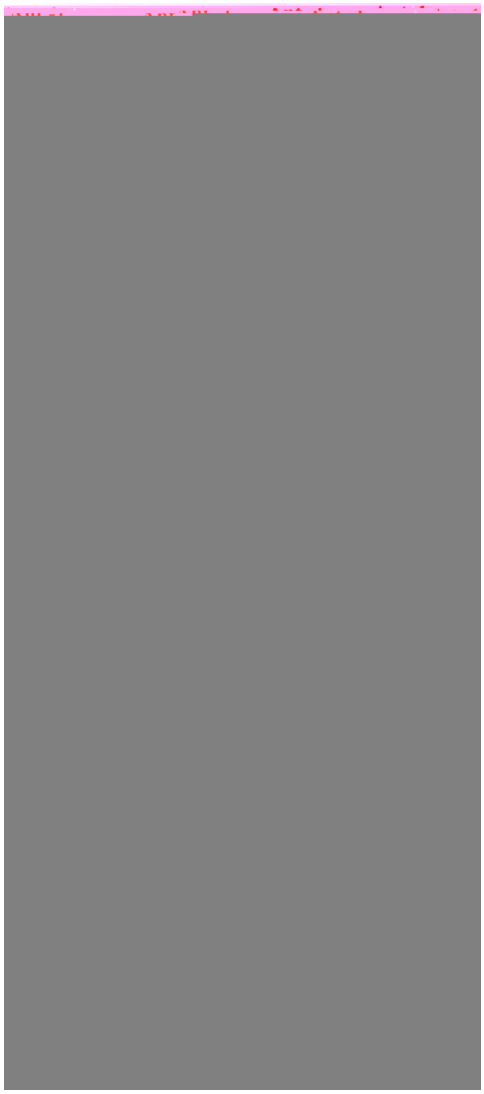

Fig. 7 *MIMO antenna designs in measurement*
(a) Prototypes of fabricated MIMO antennas of Case 1 (left) and Case 2 (right), ***(b)*** Measured *S*-parameters for Case 1, ***(c)*** Measured *S*-parameters for Case 2

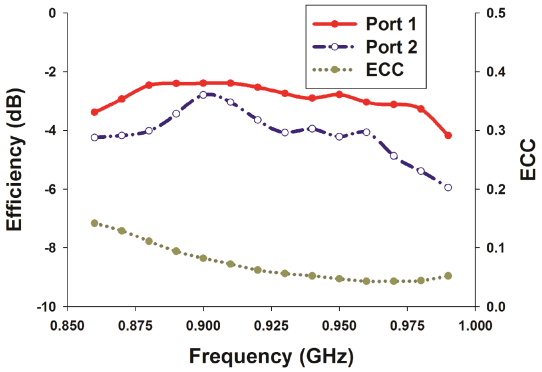

Fig. 8 *Measured total efficiency and ECC for Case 1*

can be expected from the fact that Mode 1 excited by Antenna 1 has a lower quality factor than Mode 2 excited by Antenna 2, as indicated in Fig. 1*b*. The ECC values are calculated by using measured 3D radiation patterns under the assumption of isotropic channel environment (same likelihood of impinging waves from all directions) in the anechoic chamber [29], and they are <0.15 in the operating frequency band. These values are much smaller than the usual criteria of 0.5 in mobile applications.

To better understand the diversity performance, the measured radiation patterns at 0.9 GHz are shown in Fig. 9 for Case 1. Figs. 9*a* and *b* give the radiation patterns in the *xy*- and *xz*-planes of

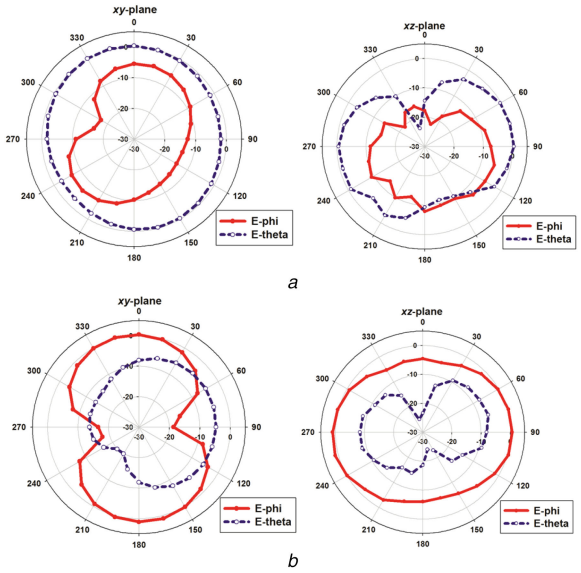

Fig. 9 *Measured radiation patterns for MIMO antennas of Case 1*
(a) *xy* and *xz* planes of Antenna 1, ***(b)*** *xy* and *xz* planes of Antenna 2

Antennas 1 and 2, respectively. First, the phi-polarised electric fields are compared. In the *xy*-plane, E_φ in Fig. 9*b* is much stronger than that in Fig. 9*a*. In the *xz*-plane, E_φ is omnidirectional in Fig. 9*b*, while it is not in Fig. 9*a*. Next, the theta-polarised electric field is then compared. In the *xy*-plane, E_θ is omnidirectional in Fig. 9*a*, but it is not in Fig. 9*b*. In the *xz*-plane, E_θ in Fig. 9*a* is much stronger than that in Fig. 9*b*. Therefore, Antenna 1 is mainly radiating as a dipole along the *z*-axis, and Antenna 2 primarily acts as a dipole along the *y*-axis. It is obvious that the radiation patterns are orthogonal to each other, which explains the low ECC values.

The above studies are based on the measurement results in the free space, however, in practice the antennas are exposed to the user effect, resulting in reduced efficiency due to mismatch and extra loss. Since the proposed antennas are radiating through the metal rim, which the users are directly touching, user scenarios can be of interest to observe. Therefore, the hand effect for the proposed MIMO antennas in Case 1 is evaluated by using a personal digital assistants (PDA) hand phantom (see Fig. 10*a*). Note that the position of the mobile device and the material properties of the phantom satisfy the measurement method of CTIA [30]. The *S*-parameters are shown in Fig. 10*b*, and it can be observed that the bandwidths and isolation are not greatly affected. However, the measured total efficiencies of both antennas are greatly reduced, as shown in Fig. 10*c*. Compared with the results in the free space, the average efficiency of Antenna 1 is reduced from −2.7 to −6.7 dB, with a degradation of 4 dB. For Antenna 2, on the other hand, the average efficiency is decreased from −4.1 to −10.4 dB, with a degradation of 6.3 dB. Furthermore, ECC values with the hand effect range from 0.02 to 0.18, and the slight difference from those in Fig. 8 can be caused by the alteration of the current distributions due to the proximity of the PDA hand. Therefore, the hand effect from users mainly affect the radiation efficiencies of the proposed antennas due to power absorption, but the efficiency degradation is still in acceptable range [3, 31].

5 Conclusion

A simple and efficient MIMO antenna design technique is proposed by utilising unbroken metal rims to achieve high isolation and low ECC performance. Quasi-degenerate and orthogonal modes of the unbroken metal rim are excited by a feeding structure with a series inductor so that the resonant frequency of the feeding is equal to the operating frequency and that of the characteristic modes. High isolation (about −10 dB) and low ECC (<0.2) can be obtained within compact size by exciting quasi-degenerate and orthogonal modes of the unbroken metal rims. Simulation and measurement results show good agreement, and good antenna performance and diversity performance are obtained. Furthermore,

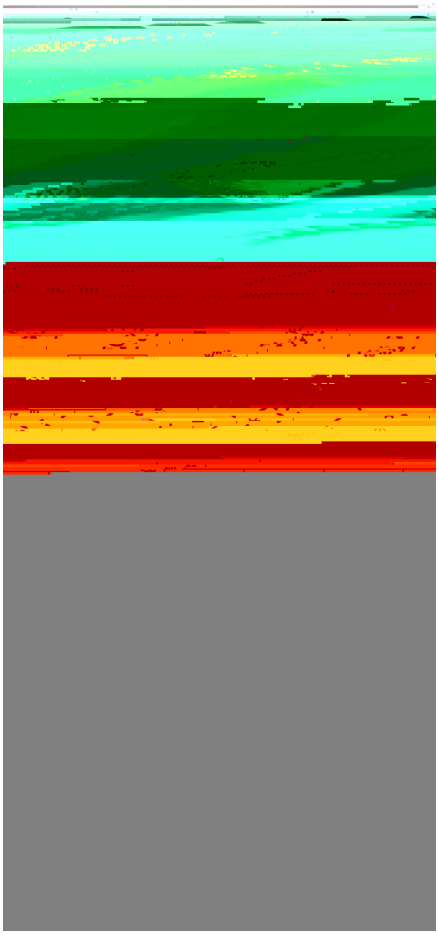

Fig. 10 *User scenarios in measurement for MIMO antennas of Case 1*
(a) PDA hand, ***(b)*** Measured *S*-parameters (PDA hand), ***(c)*** Measured total efficiencies and ECC values (PDA hand)

the hand effect is also discussed. This paper provides candidate antenna designs for both single antenna and MIMO antennas in the presence of the unbroken metal rims. Further research is on-going to meet more stringent requirements.

6 Acknowledgments

This work was supported by the ICT R&D program of MSIP/IITP, Republic of Korea (grant no. 2013-0-00401), ground radiation technique for mobile devices).

7 References

[1] Guo, Q., Mittra, R., Lei, F., *et al.*: 'Interaction between internal antenna and external antenna of mobile phone and hand effect', *IEEE Trans. Antennas Propag.*, 2012, **61**, (2), pp. 862–870
[2] Yuan, B., Cao, Y., Wang, G., *et al.*: 'Slot antenna for metal-rimmed mobile handsets', *IEEE Antennas Wirel. Propag. Lett.*, 2012, **11**, pp. 1334–1337
[3] Hsu, C.-K., Chung, S.-J.: 'Compact multiband antenna for handsets with a conducting edge', *IEEE Trans. Antennas Propag.*, 2015, **63**, (11), pp. 5102–5107
[4] Ban, Y.-L., Qiang, Y.-F., Chen, Z., *et al.*: 'A dual-loop antenna design for hepta-band WWAN/LTE metal-rimmed smartphone applications', *IEEE Trans. Antennas Propag.*, 2015, **63**, (1), pp. 45–58
[5] Wong, K.-L., Huang, C.-Y.: 'Triple-wideband open-slot antenna for the LTE metal-framed tablet device', *IEEE Trans. Antennas Propag.*, 2015, **63**, (12), pp. 5966–5971
[6] Qu, L., Zhang, R., Shin, H., *et al.*: 'Performance enhancement of ground radiation antenna for Z-wave applications using tunable metal loads', *Electron. Lett.*, 2016, **52**, (22), pp. 1827–1828
[7] Liu, Y., Zhou, Y., Liu, G., *et al.*: 'Heptaband inverted-F antenna for metal-rimmed mobile phone applications', *IEEE Antennas Wirel. Propag. Lett.*, 2015, **15**, pp. 996–999
[8] Wong, K.-L., Tsai, C.-Y.: 'IFA-based metal-frame antenna without ground clearance for the LTE/WWAN operation in the metal-casing tablet computer', *IEEE Trans. Antennas Propag.*, 2016, **64**, (1), pp. 53–60
[9] Qu, L., Zhang, R., Shin, H., *et al.*: 'Mode-controlled wideband slot-fed ground radiation antenna utilizing metal loads for mobile applications', *IEEE Trans. Antennas Propag.*, 2016, **65**, (2), pp. 867–872
[10] Sibille, A., Oestges, C., Zanella, A.: '*MIMO: from theory to implementation*' (Academic Press, San Diego, CA, 2011)
[11] Lau, B.K., Andersen, J.B.: 'Simple and efficient decoupling of compact arrays with parasitic scatters', *IEEE Trans. Antennas Propag.*, 2011, **60**, (2), pp. 464–472
[12] Qu, L., Zhang, R., Kim, H.: 'Decoupling between ground radiation antennas with ground-coupled loop-type isolator for WLAN applications', *IET Microw. Antennas Propag.*, 2016, **10**, (5), pp. 546–552
[13] Li, Z., Du, Z., Takahashi, M., *et al.*: 'Reducing mutual coupling of MIMO antenna with parasitic elements for mobile terminals', *IEEE Trans. Antennas Propag.*, 2012, **60**, (2), pp. 473–481
[14] Kwon, D., Lee, S.-J., Kim, J.-W., *et al.*: 'An eight-element compact low-profile planar MIMO antenna using LC resonance with high isolation', *J. Electromag. Eng. Sci.*, 2016, **16**, (3), pp. 194–197
[15] Chen, S.-C., Wang, Y.-S., Chung, S.-J.: 'A decoupling technique for increasing the port isolation between two strongly coupled antennas', *IEEE Trans. Antennas Propag.*, 2008, **56**, (12), pp. 3650–3658
[16] Tang, X., Mouthaan, K., Coetzee, J.C.: 'Tunable decoupling and matching network for diversity enhancement of closely spaced antennas', *IEEE Antennas Wirel. Propag. Lett.*, 2012, **11**, pp. 268–271
[17] Li, H., Miers, Z.T., Lau, B.K.: 'Design of orthogonal MIMO handset antennas based on characteristic mode manipulation at frequency bands below 1 GHz', *IEEE Trans. Antennas Propag.*, 2014, **62**, (5), pp. 2756–2766
[18] Zhang, S., Zhao, K., Ying, Z., *et al.*: 'Investigation of diagonal antenna-chassis mode in mobile terminal LTE MIMO antennas for bandwidth enhancement', *IEEE Antennas Propag. Mag.*, 2015, **57**, (2), pp. 217–228
[19] Won, J., Jeon, S., Nam, S.: 'Identifying the appropriate position on the ground plane for MIMO antennas using characteristic mode analysis', *J. Electromag. Eng. Sci.*, 2016, **16**, (2), pp. 119–125
[20] Zachary, M., Hui, L., Kiong, L.B.: 'Design of bezel antennas for multiband MIMO terminals using characteristic modes'. Proc. 8th Eur. Conf. Antennas Propag, 2014
[21] Deng, C., Feng, Z., Hum, S.V.: 'MIMO mobile handset antenna merging characteristic modes for increased bandwidth', *IEEE Trans. Antennas Propag.*, 2016, **64**, (7), pp. 2660–2667
[22] Qu, L., Lee, H., Shin, H., *et al.*: 'MIMO antennas using controlled orthogonal characteristic modes by metal rims', *IET Microw. Antennas Propag.*, 2017, **11**, (7), pp. 1009–1015
[23] Zhao, K., Zhang, S., Ishimiya, K., *et al.*: 'Body-insensitive multimode MIMO terminal antenna of double-ring structure', *IEEE Trans. Antennas Propag.*, 2015, **63**, (5), pp. 1925–1936
[24] Harrington, R.F., Mautz, J.R.: 'Theory of characteristic modes for conducting bodies', *IEEE Trans. Antennas Propag.*, 1971, **19**, (5), pp. 622–628
[25] Fabrés, M.C.: 'Systematic design of antennas using the theory of characteristic modes'. Ph.D. dissertation, Electrical Engineering, Technical University of Valencia, Valencia, Spain, 2007
[26] Vainikainen, P., Ollikainen, J., Kivekas, O., *et al.*: 'Resonator-based analysis of the combination of mobile handset antenna and chassis', *IEEE Trans. Antennas Propag.*, 2002, **50**, (10), pp. 1433–1444
[27] Qu, L., Zhang, R., Lee, H., *et al.*: 'Compact triple-band ground radiation antenna using two inner rectangular loops enclosed by two outer loops', *Electron. Lett.*, 2016, **52**, (10), pp. 790–792
[28] Huang, L., Schroeder, W.L., Russer, P.: 'Estimation of maximum attainable antenna bandwidth in electrically small mobile terminals'. Proc. 36th Eur. Microw. Conf., Manchester, UK, 2006
[29] Vaughan, R.G., Andersen, J.B.: 'Antenna diversity in mobile communications', *IEEE Trans. Veh. Technol.*, 1987, **36**, (4), pp. 149–172
[30] Test Plan for Mobile Station Over the Air Performance CTIA Revision 3.1, January 2011
[31] Zhang, S., Zhao, K., Ying, Z., *et al.*: 'Adaptive quad-element multi-wideband antenna array for user-effective LTE MIMO mobile terminals', *IEEE Trans. Antennas Propag.*, 2013, **61**, (8), pp. 4275–4283